Whole-exome sequencing identification of a recurrent *CRYBB2* variant in a four-generation Chinese family with congenital nuclear cataracts

DOUDOU CHEN[1-3] and SIQUAN ZHU[1-4]

[1]Eye School of Chengdu University of Traditional Chinese Medicine, Chengdu, Sichuan 610075; [2]Department of Ophthalmology, Ineye Hospital of Chengdu University of Traditional Chinese Medicine; [3]Key Laboratory of Sichuan Province Ophthalmopathy Prevention & Cure and Visual Function Protection, Chengdu University of Traditional Chinese Medicine, Chengdu, Sichuan 610032; [4]Department of Ophthalmology, Beijing Anzhen Hospital, Capital Medical University, Beijing 100006, P.R. China

Received January 14, 2021; Accepted August 19, 2021

DOI: 10.3892/etm.2021.10810

Abstract. Congenital cataracts is the most common cause of visual impairment and blindness in children. Although there have been extensive studies into the pathogenesis of congenital cataracts, the pathogenic mechanism underlying the recurrent variant *CRYBB2*:c.62T>A(p.I21N) has not been previously reported. Thus, the present study aimed to use whole-exome sequencing (WES) to identify potential genetic variants and investigate how they may have induced the occurrence of cataracts in a four-generation Chinese family with congenital nuclear cataracts. The medical history of this family was recorded and WES was conducted for one proband. Sanger sequencing was used to verify the presence of the putative variant in all participants. PolyPhen-2, SIFT and ProtScale were used to analyze the effect of the identified variants on protein function and hydrophobicity, and Pymol was used to show the structure of the wild-type (Wt) and mutant β-crystallin B2 (*CRYBB2*) protein. Full-length Wt-*CRYBB2* or mutant-*CRYBB2* (I21N-*CRYBB2*) were fused to green fluorescent protein (GFP), and the recombinant plasmids were transfected into HeLa cells. Reverse transcription-quantitative PCR and western blotting were used to detect the expression levels of *CRYBB2* mRNA and protein. Immunofluorescence and flow cytometry analyses were used to detect protein localization and apoptosis, respectively. A recurrent variant *CRYBB2*:c.62T>A(p.I21N) was identified in a four-generation Chinese family with congenital nuclear cataracts. Multiple-sequence alignment of CRYBB2 demonstrated that codon 21 was highly conserved. Pymol revealed that the structure of the I21N-*CRYBB2* protein was distinct from that of Wt-*CRYBB2*. PolyPhen-2 predicted that it had a variant provean score 1.0, suggesting it was 'probably damaging', and SIFT predicted it had a variant provean score of -5.113, indicating it was 'deleterious'. ProtScale indicated that the hydrophobicity of the mutation site was significantly reduced. The protein expression levels of the I21N-*CRYBB2* were decreased compared with the Wt-*CRYBB2*. Immunofluorescence analysis revealed that the variant I21N-*CRYBB2* protein tended to accumulate around the nucleus, and flow cytometry analysis indicated that it increased cell apoptosis. Furthermore, I21N-*CRYBB2* induced the activation of the unfolded protein response (UPR). In conclusion, a pathogenic variant of *CRYBB2*:c.62T>A(p.I21N) was identified via WES in a four-generation Chinese family with congenital nuclear cataracts. Through biological analysis, it was found that the variant induced abnormal protein aggregation, activated the UPR and triggered excessive cell apoptosis, which may lead to the occurrence of congenital nuclear cataracts in this family.

Correspondence to: Dr Siquan Zhu, Eye School of Chengdu University of Traditional Chinese Medicine, 37 Twelve Bridge Road, Chengdu, Sichuan 610075, P.R. China
E-mail: siquan_zhu01@sina.com

Abbreviations: WES, Whole-exome sequencing; CRYBB2, β-crystallin B2; InDel, insertion or deletion; BCVA, best-corrected visual acuity; Wt-CRYBB2, wild-type-CRYBB2; GFP, green fluorescent protein; UPR, unfolded protein response; BiP, binding immunoglobulin protein; Ire1, inositol-requiring enzyme 1; HSPA5, heat shock protein family A (Hsp70) member 5; Xbp1, X-box-binding protein

Key words: congenital cataracts, cataract genetics, WES, CRYBB2, autosomal dominant, variant, mutation

Introduction

Congenital cataracts are a common heterogeneous disease that causes variable degrees of visual impairment and blindness in partially affected children, and the etiology involves both genetic and environmental components (1). Congenital cataracts typically appear as opacification in any position of the lens before or after birth. Any obstruction in the visual axis that is left untreated may lead to permanent impairment of vision or even blindness, even if it is removed at a

later stage (2). Congenital cataracts may manifest as isolated cataracts or syndrome-associated cataracts (3). Worldwide, the prevalence of congenital cataracts in live births ranges from 1-15/10,000 children, and it is responsible for 10-30% of cases of blindness in children (4).

The causes of congenital cataracts include gene defects, environmental factors, chromosomal abnormalities, metabolic disorders and perinatal infections (1,2,4). Inherited cataracts, caused by genetic mutations, contribute to half of all cases of congenital cataracts (2). Several gene mutations are considered to participate in the pathology of congenital cataracts, amongst which, mutations of the crystallin gene are the most widely recorded, and account for ~1/2 of all reported mutations associated with congenital cataracts (5). Mutations in β-crystallin B2 (*CRYBB2*) that cause congenital cataracts are commonly reported (6). At present, 22 mutations in the *CRYBB2* gene have been identified (7). There are also several studies on the underlying pathological mechanisms of the *CRYBB2* mutations that lead to congenital cataracts (8,9). Although *CRYBB2*:c.62T>A(p.I21N) is a recurrent variant, its pathogenic mechanism has not been previously reported to the best of our knowledge.

Implementation of genetic testing using whole-exome sequencing (WES) has permitted the streamlining of the process of identifying pathogenic genetic variants, especially when it is widely used in the diagnosis of a variety of single-gene diseases (10). In the present study, WES was used to examine the genetic cause in a four-generation Chinese family with congenital nuclear cataracts. In addition, the pathological mechanism of *CRYBB2*:c.62T>A(p.I21N) was evaluated *in vitro*. This variant has been identified in one other family (11), but the phenotype was completely distinct from the family examined in the present study. Patients in the aforementioned study were born with regular nuclear cataracts in both eyes (11). It was hypothesized that this site may be a mutation hotspot, hence it is essential to investigate the mechanism via which this variant may cause congenital cataracts. This may provide a reference and possible therapeutic target for gene therapy of congenital cataracts in the future.

Materials and methods

Subjects. A four-generation Chinese family with congenital nuclear cataracts and 100 healthy controls (age range, 20-55 years, 50 women, 50 men) were recruited from July 2018 to July 2019 from the Yin Hai Eye Hospital (Chengdu, China). There were a total of 21 family members (12 males, 9 females; age range, 2-77 years; average age, 33.4±20.7 years) in this family, of which, 8 were affected and 13 were unaffected. Except for the member I. 1 who passed away, peripheral venous blood was collected from all remaining family members. All participants signed informed consent forms or this was signed by the guardian, and the study was performed in accordance with the Declaration of Helsinki (12). The pedigree medical history was recorded and clinical examinations were performed. The Institutional Review Board of Chengdu University of Traditional Chinese Medicine approved the present study (approval no. CMEC2010-21).

DNA collection and whole exome sequencing analysis. Paired-end sequencing for reads of 150 bp was performed using the Illumina X-10 platform (Illumina, Inc.). Peripheral venous blood was extracted from all participants using a vacuum blood collector (BD Biosciences). DNA was extracted using a DNA Extraction kit (cat. no. 69504; Qiagen China Co., Ltd.) and purified using a DNA Purification kit (cat. no. K0512; Invitrogen; Thermo Fisher Scientific, Inc.) according to the manufacturer's protocol. The purity and quantity of DNA samples were subsequently measured using the NanoDrop 2000 spectrophotometer (Thermo Fisher Scientific, Inc.) and agarose gel electrophoresis. A high-quality genomic DNA sample was broken using Covaris Technologies (200 and 300 bp), as previously described (13). The sample was then prepared using a Truseq DNA Sample Preparation kit (Illumina, Inc.,) and captured using a SureSelect all exons Enrichment kit (Agilent Technologies, Inc.). Captured products were exposed to an Agilent 2100 Bioanalyzer (14) to detect the mass concentration of the library, and the final library concentration was 5.14 ng/μl. Agarose gel electrophoresis detected clear and slightly diffused bands at 200-500 bp, indicated that the library had been successfully constructed.

The raw data were filtered to obtain clean reads according to the following steps: i) Removing reads containing sequencing adapter; ii) removing reads whose low-quality base ratio (base quality ≤5) is >50%; and iii) removing reads whose unknown base ('N' base) ratio is >10%. Statistical analysis of data and downstream bioinformatics analysis were performed on this filtered, high-quality data, referred to as the 'clean data'. The alignment software, Burrows-Wheeler Aligner (version, 0.7.17) (15), was used to align the clean data to the human reference genome (GRCh37/HG19). The Picard tool (version, 1.119) (16) was used to remove duplicate reads, and GATK (version, 3.8) (17) was used for local realignment and base quality recalibration.

Processing of sequencing data. In order to ensure high-quality sequencing data, a strict data quality control system was set up for use throughout the analytical process. Data were further annotated using ANNOVAR (version, 2.3) (18) and evaluated using multiple databases, including The 1000 Genomes Project (ncbi.nlm.nih.gov/variation/tools/1000genomes), ESP6500.exon.program(evs.gs.washington.edu/EVS),dbSNP(ftp://ftp-trace.ncbi.nih.gov/snp/organisms), ExAC (exac.broadinstitute.org), Inhouse (MyGenostics), HGMD (hgmd.cf.ac.uk/ac/index.php), OMIM (omim.org/), ClinVar (ncbi.nlm.nih.gov/clinvar) and gnomAD (gnomad.broadinstitute.org/about). SIFT (19), PolyPhen-2 (20), MutationTaster (21) and GERP++ (22) were used to predict the effect of variations on protein function. During data analysis, the variations were selected according to the following conditions: i) Variants that are reported in dbSNP v141; ii) the subset of variants with MAF <1% in The 1000 Genome Project; iii) subset of coding non-synonymous single nucleotide polymorphisms (SNPs) with SIFT score <0.05; or iv) intergenic variants with GERP++ score >2. The identified variations were assessed according to the variant interpretation guidelines of the American College of Medical Genetics and Genomics (ACMG) (23,24). Next, the putative variations in the affected members, the relatives and the healthy controls were compared with the OMIM database, as well as with previously published literature (5,9).

Sanger sequencing. A pair of primers were designed by Thermo Fisher Scientific, Inc.; the sequences were: *CRYBB2* forward, 5'-CCTTCAGCATCCTTTGGGTTCTCT-3' and

reverse, 5'-GCAGTTCTAAAAGCTTCATCAGTC-3'. Sanger sequencing was performed on all family members and control participants using an ABI 3730 Genetic analyzer (Applied Biosystems; Thermo Fisher Scientific, Inc.) according to the manufacturer's protocol.

Bioinformatics analysis. Pymol (version, 2.5; https://pymol.en.softonic.com/; Schrödinger, LLC) (25) showed the protein structure of wild-type (Wt)-*CRYBB2* and mutant (I21N)-*CRYBB2*, and the potential functional influence of this amino acid change detected from the variant was calculated using PolyPhen-2 (20) and SIFT (19). ProtScale (version 3.0; web.expasy.org/protscale) was used to evaluate protein hydrophobicity.

Cell culture and transfection. HeLa cells were obtained from the American Type Culture Collection, and cultured in DMEM (standard low-glucose DMEM, 1 g/l; cat. no. 11054001; Gibco; Thermo Fisher Scientific, Inc.) supplemented with 10% FBS (cat. no. 10100147; Gibco; Thermo Fisher Scientific, Inc). Cells were maintained at 37˚C in a humidified incubator with 5% CO_2. Subsequently, cells in the logarithmic growth phase were seeded into a 6-well plate, and the seeding density reached 70-90% for transfection at room temperature. A total of 2 μg Wt- or I21N-CRYBB2 plasmid/well were transfected into cells using Lipofectamine® 3000 (Invitrogen; Thermo Fisher Scientific, Inc.) according to the manufacturer's protocol, at 37˚C for 48 h. When the concentration of transfected cells reached 80%, the transfected cells were analyzed.

Reverse transcription-quantitative (RT-q)PCR. To determine the relative expression of the empty vector, Wt- and I21N-CRYBB2 in transfected cells, RT-qPCR was performed. Total RNA was extracted using TRIzol® reagent (Invitrogen; Thermo Fisher Scientific, Inc.), qPCR SYBR® Green Master Mix (Vazyme Biotech, Co., Ltd.) and the RNA was reverse transcribed into cDNA using a QuantiTect Reverse Transcription kit (cat. no. 205313, Qiagen China Co., Ltd.), according to the manufacturer's protocol. qPCR was performed using a PCR amplifier (26). The method of gene quantification used was $2^{-\Delta\Delta Cq}$ as previously described (27). PCR primers were designed by Invitrogen (Thermo Fisher Scientific, Inc.) as follows: *CRYBB2* forward, 5'-GTAGCCAGGATTCTGCCATAGGAA-3' and reverse, 5'-GTGCCCTCTGGAGCATTTCATAGT-3'; *GAPDH* forward, 5'-TTCCGAGTTCCTGTCCCTAATG-3' and reverse, 5'-GCCTCCTTCACCTTCTGCTTG-3'. qPCR was performed using the FTC2000 (Funglyn Biotech). Samples were set up in 50 μl final volumes containing 6 μl 5X PCR buffer, 0.6 μl 2X primers (25 pmol/μl), 0.3 μl probe (25 pmol/μl) or 0.3 μl SYBR-Green, 1 μl dNTPs (10 mM), 0.3 μl Taq enzyme (5 U/μl), 3 μl $Mg2^+$ (25 mM), 1 μl template and 17.2 μl DEPC water (Sigma-Aldrich; Merck KGaA). Thermocycling conditions were as follows: Initial denaturation at 94˚C, followed by 40 cycles of 20 sec at 94˚C and 30 sec at 60˚C. The relative expression was calculated based on the expression of GAPDH.

Western blotting. After cells were lysed in a mix containing SDS Lysis Buffer (cat. no. p0013; Beyotime Institute of Biotechnology) and protease inhibitors (Sigma-Aldrich; Merck KGaA), proteins were extracted. Proteins were quantified using a BCA Protein Assay kit (cat. nos. CW0014S and CWBIO). A total of 25 μg of each protein sample was loaded per lane on a 12% SDS-gel, resolved using SDS-PAGE and transferred to PVDF membranes. The membrane was then incubated with the following antibodies: anti-green fluorescent protein (GFP; cat. no. ab290; Abcam; 1:1,000), anti-GAPDH (cat. no. ab8245; Abcam; 1:1,000) and anti-BiP/HSPA5 (cat. no. ab21685; Abcam; 1:1,000), at 4˚C overnight. Subsequently, the membranes were then incubated with the secondary antibody horseradish peroxidase (HRP) Goat anti-Rabbit IgG antibody (cat. no. ab6721; Abcam, 1:5,000) or (HRP) Goat anti-Mouse IgG antibody (cat. no. ab6721; Abcam; 1:5,000) diluted with 5% skimmed milk powder blocking solution for 1 hour at room temperature. Signals were visualized using an ECL reagent (Thermo Fisher Scientific, Inc.), the membranes were subsequently scanned and densitometry analysis was performed. Protein band intensities were quantified using ImageJ software (version, 1.8.0_172; National Institutes of Health).

Immunofluorescence and apoptosis analysis. The transfected cells were washed with PBS three times, fixed with 100% pre-cooled acetone (stored at 4˚C) for 10 min at room temperature, washed again with PBS three times and then stained with DAPI for 10 min at room temperature. The slides were sealed and cells were observed using a confocal microscope (magnification, x200). The number of aggregated cells was counted using ImageJ software (version, 1.8.0_172; National Institutes of Health).

Apoptosis was observed using Hoechst 33342 staining. After 24 h, the cells transfected with Wt- and I21N-*CRYBB2* plasmids were placed into a 6-well plate at $2x10^5$/well and cultured for another 24 h in DMEM supplemented with 10% FBS. When the cell seeding density reached 70-90%, Hoechst 33342 was added to the wells at room temperature for 10 min, and the number of apoptotic nuclei were counted using a confocal microscope (magnification, x200). Cells transfected with Wt- or I21N-*CRYBB2* plasmid were transferred to 6-well plates, 400 μM H_2O_2 was used to induce stimulation, and an apoptosis assay was then performed on a flow cytometer (Attune NxT; Thermo Fisher Scientific, Inc.) using Annexin V-FITC/PI Apoptosis Detection kit (cat. no. A211-01/02; Vazyme Biotech Co., Ltd.) according to the manufacturer's instructions. The cells apoptotic rate was calculated by the percentage of early plus late apoptotic cells.

Molecular analysis of UPR-related genes induced by mutant crystallin. RT-PCR was performed for X-box-binding protein (Xbp1) splicing and to detect the expression levels of other UPR-related genes, as previously described. The following primers were used: *Xbp1* forward, 5'-GAACCAGGAGTTAAGAACACG-3' and reverse, 5'-AGGCAACAGTGTCAGAGTCC-3' for *Xbp1* splicing; heat shock protein family A (Hsp70) member 5 (*HSPA5*) forward, 5'-CCAAGAGAGGGTTCTTGAATCTCG-3' and reverse, 5'-AGGCAACAGTGTCAGAGTCC-3'; DNA damage-inducible transcript 3 (*DDIT3*) forward, 5'-AGCCGTTCATTCTCTTCAG-3' and reverse, 5'-CCTCACTCTCCAGATTCCA-3'; *GAPDH* forward, 5'-AGGCTGTTG

TCATACTTCTC-3' and reverse, 5'-CATCACCATCTTCCA GGAG-3'; inositol-requiring enzyme 1 (*Ire1*) forward, 5'-CGG TCAGGAGGTCAATAACA-3' and reverse, 5'-GGACAGGCT CAATCAAATGG-3'; and β2-microglobulin, forward, 5'-GGA TGGATGAAACCCAGACACATAG-3' and reverse, 5'-CGG GCATTCCTGAAGCTGA-3'.

Statistical analysis. Statistical analysis was performed using SPSS 23.0 software (IBM Corp.). Each experiment was repeated ≥3 times. The percentage of cells with aggregates was calculated from 200 positively transfected cells in 10 random viewing fields. The numbers of apoptotic nuclei were counted in five random viewing fields. All data are expressed as the mean ± SD. One-way ANOVA and Bonferroni multiple comparison were used to test the differences between three groups. $P<0.05$ was considered to indicate a statistically significant difference.

Results

Clinical information of the patients. According to the sequencing and genetic characteristics, the family enrolled in the present study possessed an autosomal dominant inheritance pattern (Fig. 1A), the proband IV.1 was a 4-year-old boy who was found to have congenital binocular nuclear cataracts at birth and underwent cataract phacoemulsification without intraocular lens implantation at the age of 2 months (Fig. 1B). At the age of 2 years, he underwent binocular sequential intraocular lens implantation. However, the left eye developed secondary glaucoma and corneal ulcers within 2 years after cataract surgery. At the age of 4 years, he underwent a left eye prosthesis implantation operation. At present, his best corrected visual acuity (BCVA) in his right eye is 0.2, and his intraocular pressure is normal. He has slight nystagmus and esotropia without fundus abnormalities. Family member IV.2 was the half-sister of the proband, who also presented with binocular nuclear cataracts after birth. She underwent binocular cataracts surgery at the age of 2 months and, at present, has a bilateral aphakic eye. She also has esotropia and nystagmus. The mother (III.1) of the proband presented with binocular nuclear cataracts at birth and underwent binocular cataracts surgery with intraocular lens implantation at the age of 2 years. Currently, her BCVA is 0.02 in the right eye and 0.1 in the left eye, and shows notable nystagmus and esotropia without any fundus abnormalities. The grandmother (II.1) of the proband also had binocular nuclear cataracts at birth, and underwent binocular cataracts removal surgery at the age of 12 years without intraocular lens implantation; her BCVA is 0.01 in the right eye and 0.06 in the left eye, and shows obvious nystagmus and esotropia without any fundus abnormalities. Family member IV.3 is a cousin of the proband, also had binocular nuclear cataracts at birth, and underwent binocular cataracts removal at the age of 2 years without intraocular lens implantation. She is still aphakic. Her BCVA is 0.02 in the right eye and 0.06 in the left eye. However, her half-brother (IV.4) does not have cataracts. Her mother (III.2) also presented with binocular nuclear cataracts at birth, and underwent binocular cataracts removal surgery with implantation of an intraocular lens at the age of 4 years. Her BCVA was 0.1 in the right eye and 0.06 in the left eye. She also exhibited esotropia and nystagmus without fundus abnormalities. Family member II.2 is the mother of III.2, and also presented with binocular nuclear cataracts at birth. This individual underwent binocular cataract extraction without intraocular lens implantation at the age of 11 years. Her BCVA was 0.02 in the right eye and 0.01 in the left eye. She remained aphakic, showing obvious nystagmus and esotropia without any fundus abnormalities. Specific clinical information is presented in Table I.

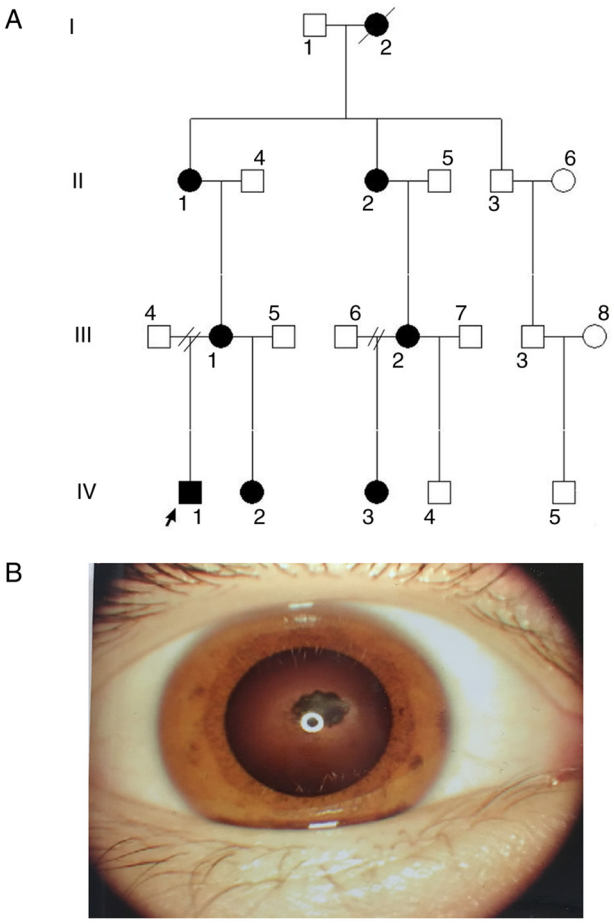

Figure 1. Family pedigree and cataract phenotype of proband. (A) Pedigree of the family. The squares and circles represent men and women, respectively. Solid and hollow indicate wild-type and variant individuals, respectively. The solid black arrow indicates the proband (IV.1), and the diagonal line indicates the deceased family member. (B) Image of the lens of the proband (IV.1).

Sequencing results and mutation analysis. An average of 98.9025 Mb raw bases were obtained. After filtration, an average of 14.4726G clean reads were obtained. The clean reads had a high-quality value (Q30, 0.93) and the average G and C basepair content was 48.66%. The results of the analysis of the clean data suggested that the mapping rate on genome was 99.61%, the average sequencing depth was 127.97 and the coverage of the sequencing depth ≥20X was 97.65%. Thus, the target area had been effectively covered, and the sequencing quality was high (Table II).

After bioinformatics analysis, 112,986 SNPs were identified in the proband, 99.25% of which were annotated in dbSNP and 94.06% were annotated in The 1000 Genomes Project database. Of these, 842 SNPs were novel. Amongst all SNPs, 11,046 were synonymous, 10,293 were missense, 32 were stop-loss,

Table I. Clinical information of patients in this families.

Patient	Age, years	Sex	BCVA (R/L)	Type of cataracts	Age of removal cataract	IOL v. aphakia	Refractive error at age examined (R, L)	Nystagmus	Strabismus subtype	Fundus anomalies
IV.1	4	M	0.2/-	Bilateral nuclear cataract	2 month	IOL/Prosthetic eye	+4.00DS/-2.00DCx10, -	Ophthalmic nystagmus	Esotropia	NA
IV.2	2	F	NA/NA	Bilateral nuclear cataract	2 month	Aphakia	NA/NA	Ophthalmic nystagmus	Esotropia	NA
IV.3	8	F	0.02/0.06	Bilateral nuclear cataract	2 years	Aphakia	+19.00DS/-0.50DCx60 +22.50DS/-1.50DCx30	Ophthalmic nystagmus	Esotropia	Normal
III.1	30	F	0.02/0.1	Bilateral nuclear cataract	2 years	IOL	-0.75DS/-0.50DCx180 -2.00DS/-2.75DCx10	Ophthalmic nystagmus	Esotropia	Normal
III.2	35	F	0.1/0.06	Bilateral nuclear cataract	4 years	IOL	-2.50DS/-1.50DCx170 -1.50DS/-1.50DCx110	Ophthalmic nystagmus	Esotropia	Normal
II.1	53	F	0.01/0.06	Bilateral nuclear cataract	12 years	Aphakia	+17.50DS/-1.00DCx5 +16.00DS/-2.00DCx160	Ophthalmic nystagmus	Esotropia	Normal
II.2	50	F	0.02/0.01	Bilateral nuclear cataract	11 years	Aphakia	+11.25DS/0.75DCx130 +20.00DS/-1.50DCx90	Ophthalmic nystagmus	Esotropia	Normal

BCVA, best-corrected visual acuity; M, male; F, female; IOL, intraocular lens; NA, not acquire; R, right; L, left.

Table II. Quality control data statistics.

Sample	Proband
Clean reads (M)	98.90
Clean bases (G)	14.47
Q20 (%)	97.03
Q30 (%)	92.96
GC (%)	48.66
Read length (bp)	150.00
Initial bases on target	50,390,601.00
Total effective reads	82,447,708.00
Total effective bases (Mb)	11,908.75
Effective sequences on target (Mb)	6,438.89
Capture specificity (%)	54.07
Mapping rate on genome (%)	99.61
Duplicate rate on genome (%)	16.70
Mismatch rate in target region (%)	0.49
Average sequencing depth on target	127.97
Fraction of target covered ≥1x (%)	99.70
Fraction of target covered ≥4x (%)	99.43
Fraction of target covered ≥10x (%)	98.88
Fraction of target covered ≥20x (%)	97.65

Table III. Summary statistics for sequencing data.

Sample	Proband
Total SNPs	112,986
Fraction of SNPs in dbSNP (%)	99.25
Fraction of SNPs in 1000 genomes (%)	94.06
Novel	842.00
Homozygous	49,261.00
Heterozygous	63,725.00
Intron	74,427.00
5'UTRs	1,787.00
3'UTRs	3,457.00
Upstream	3,346.00
Downstream	2,736.00
Intergenic	4,437.00
Synonymous	11,046.00
Missense	10,293.00
Stop-gain	83.00
Stop-loss	32.00
Start-loss	15.00
Splicing	83.00
Total InDels	18,007.00
Fraction of InDels in dbSNP (%)	90.88
Fraction of InDels in 1000 genomes (%)	60.87
Novel	1,532.00
Homozygous	7,595.00
Heterozygous	10,412.00
Intron	14,422.00
5'UTRs	245.00
3'UTRs	674.00
Upstream	497.00
Intergenic	682.00
Frameshift	281.00
Non-frameshift insertion	143.00
Non-frameshift deletion	181.00
Stop-loss	1.00
Start-loss	1.00
Splicing	65.00

UTR, untranslated region.

83 were stop-gain, 15 were start-loss and 83 were splice-site mutations. A total of 18,007 insertion/deletions (InDels) were identified. Of these, 90.88% were listed in dbSNP and 60.87% in The 1000 Genomes Project. The number of novel InDels was 1,532. Of the overall InDels, 281 were frameshift, 1 was stop-loss, 1 was start-loss and 65 were splice-site mutations (Table III). After comparison with mutation sites in dbSNP, the 1000 Genomes Project, ExAC, OMIM, HGMD, ClinVar and gnomAD, variation sites with a frequency <0.01 were selected. Genes associated with hereditary eye diseases were analyzed and according to the ACMG guidelines (23,24), using software calculation and prediction, a causative genetic variant was obtained, *CRYBB2*:c.62T>A(p.I21N). Sanger sequencing verified that *CRYBB2*:c.62T>A (p.I21N) was found in all patients, but not in the other relatives and healthy participants (Fig. 2A). The variation and cataracts phenotype were co-segregated in this family. Multi-species sequence alignment demonstrated that the locus was highly conserved (Fig. 2B).

Bioinformatics analysis of the p.I21N variant at the protein level. The protein structure of Wt- and Mut-*CRYBB2* was predicted using Pymol (28). It was found that the variant changed the secondary structure of the protein, specifically altering a portion of the helix and folding (Fig. 3). In addition, it was predicted to cause damage when based on PolyPhen-2, with a score of 1.0 (Fig. 4A). Hydrophobicity analysis showed that the hydrophobicity of this site in the variant protein was lower than that of the Wt protein (Fig. 4B).

Differences in protein expression and effect on apoptosis. *CRYBB2* mRNA was assessed via qPCR analysis, which revealed a significantly higher transcript abundance than in empty vector-cells, and there was no difference in mRNA expression levels between Wt- and Mut-*CRYBB2* (Fig. 5A). The expression levels of the CRYBB2 proteins were further evaluated via western blotting using an anti-GFP antibody, a specific cross-reactive band was observed in transfected cells, whereas no such band was detected in empty vector-cells cell. These results demonstrated this gene, that with or without mutation, was successfully expressed in transfected cells; however, the protein expression levels of Mut-*CRYBB2* were notably lower than that of Wt-*CRYBB2* (Fig. 5B). The expression level of the fusion protein carrying GFP was observed via confocal microscopy, and it was found that the Wt-*CRYBB2* was uniformly expressed in the cytoplasm, whereas the Mut-*CRYBB2* primarily surrounded the nucleus, gathering at the nuclear membrane (Fig. 5C).

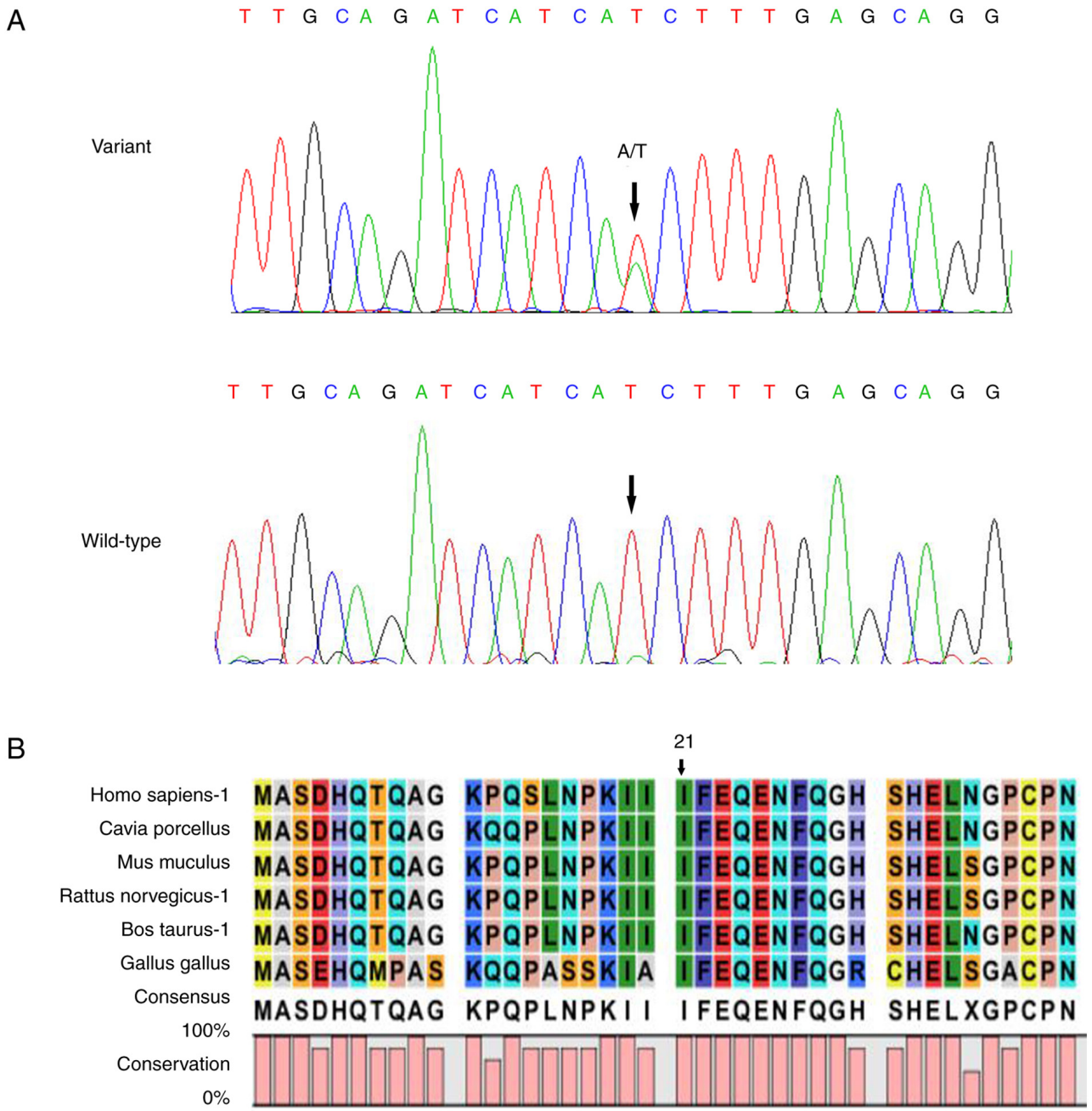

Figure 2. Sanger sequencing and multiple-sequence alignment. (A) Sanger sequencing showed that *CRYBB2*:c.62T>A (p.I21N) was detected in all variant individuals. (B) Multiple-sequence alignment showed the variant p. I21N was located within a highly conserved region. CRYBB2, β-crystallin B2.

Following nuclear staining with Hoechst 33342, it was found that the apoptotic rate of cells transfected with Wt-*CRYBB2* plasmid was not affected, but the apoptotic rate of cells transfected with the Mut-*CRYBB2* plasmid was increased (Fig. 6A). This conclusion was also verified via flow cytometry analysis; the apoptosis of cells transfected with the Mut-*CRYBB2* plasmid was increased (Fig. 6B).

UPR-associated gene expression status in cells. The UPR is a type of adaptive signal induced by abnormal accumulation of intracellular proteins (29). BiP/HSPA5 is a marker protein of the endoplasmic reticulum (ER) emergency response, and is a Hsp70 family chaperone localized in the ER lumen (30). It has been confirmed that apoptosis induced by the UPR is involved in the pathological mechanism of congenital cataracts (9). In the present study, following identification of abnormal aggregation of the variant protein, an UPR was also observed, and this may have been involved in the formation of congenital nuclear cataracts in this family. The western blotting results indicated that the expression of BiP was abnormally increased in the cells transfected with the Mut-*CRYBB2* plasmid (Fig. 7A). In addition, the expression levels of UPR-related transcription factors were also significantly increased in the Mut group, including *HSPA5*, *DDIT3* and *IRE1* (Fig. 7B-D). *IRE1* is triggered by the splicing of the Xbp1 mRNA (31), and in the present study, increased expression of *XBP1* was also observed in cells transfected with Mut-*CRYBB2* plasmids (Fig. 7E).

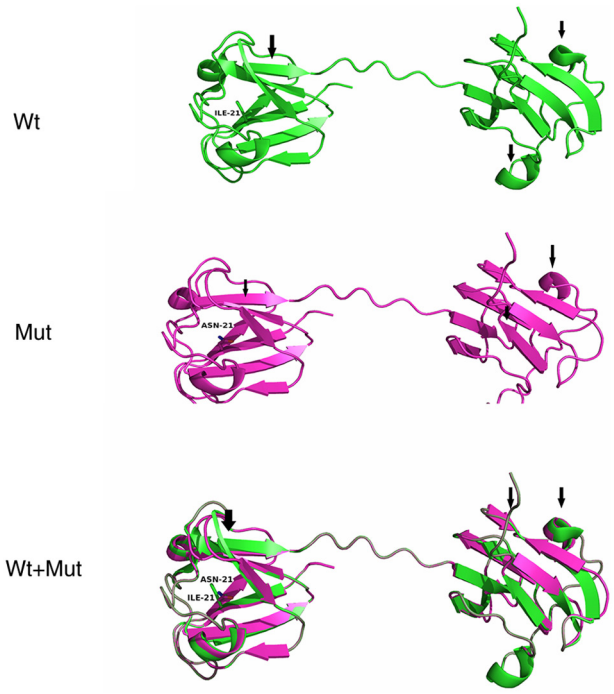

Figure 3. Structure of the CRYBB2 protein as predicted by Pymol. Green and red indicate the Wt and the variant, respectively. Pymol showed that a β-strand and an α-helix were altered in the variant protein and that the Wt and variant protein were not fully composite. CRYBB2, β-crystallin B2; Wt, wild-type; Mut, mutant.

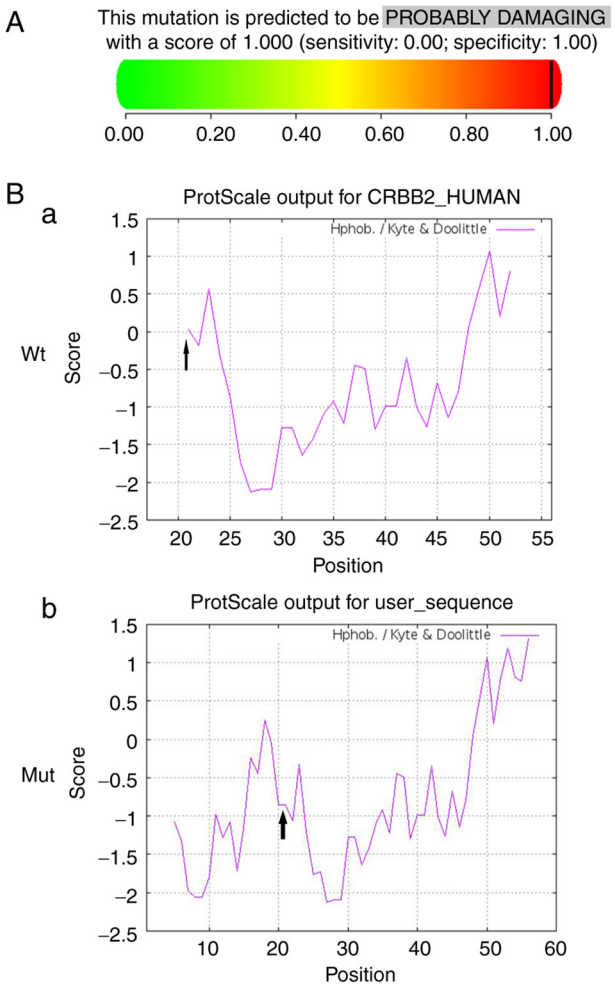

Figure 4. PolyPhen-2 evaluation and hydropathy analysis. (A) Score obtained from PolyPhen-2 analysis was 1.0, indicating that the p. I21N variant was predicted to damage the structure and function of the CRYBB2 protein. (B) Analysis of hydropathy indicated that the hydrophobicity of the variant site was lower than that of the Wt. Hydrophobicity analysis of (a) Wt and (b) Mut. Wt, wild-type; CRYBB2, β-crystallin B2; Mut, mutant.

Discussion

Congenital cataracts are a complicated heterogeneous disease, and it is generally accepted that genetic defects and environmental factors are the primary causes (32). WES is widely used to identify genetic defects in complex genetically heterogeneous diseases (33). In the present study, WES was used to identify a recurrent variant, *CRYBB2*:c.62T>A (p.I21N), in a four-generation Chinese family with congenital nuclear cataracts. The variant was found to exist in all patients, but not in other healthy relatives and the controls. There were a total of 8 affected members and 13 unaffected members in this family, according to the case records, and all patients presented with binocular nuclear cataracts at birth, and all had different degrees of esotropia and nystagmus. Congenital cataracts exhibits complex genetic heterogeneity. Although it is generally hypothesized that congenital cataracts are a single-gene disease, through a large number of clinical observations, no regular correlation between a specific gene mutation and the cataracts phenotype has been found (32,34). Therefore, it is considered that post-transcriptional modifications or other modified genes and environmental factors may also serve an important role in the occurrence of congenital cataracts. Therefore, the present study may only explain the family's congenital cataracts. Congenital cataracts in other families caused by the same mutation CRYBB2:c.62T>A (p.I21N) may exhibit alternative mechanisms. Future investigations will aim to recruit families with congenital cataracts caused by the same mutation, and compare the similarities and differences between these families.

Strabismus of certain patients with congenital cataracts develops following the occurrence of congenital cataracts, and nystagmus may be induced by low vision (35,36). In addition, the operational time of surgery for congenital cataracts has a certain impact on postoperative vision (37). In childhood, cataracts can prevent light from entering the eyes and hinder the development of the retina, resulting in deprivation of amblyopia. All patients in the present study had poor vision to a certain degree, and this was accompanied by nystagmus and esotropia. This may also be associated with the fact that cataract surgery for patients in this family was performed relatively late compared with the onset of the disease.

The *CRYBB2* gene is located on 22q11.23 and contains six exons, with the start of translation beginning in the second exon. Exons 3-6 each encode one Greek key motif (GKM). Its protein product includes 205 amino acids with a molecular weight of 23, 379 and 20 kDa. At present, congenital cataracts induced by *CRYBB2* variants have been widely reported, most of the reported *CRYBB2* variants are located in the last two exon regions (7). p.D128V in exon 6 alters the hydrophobicity and charge of the random coil region between amino acids 126-139 of the CRYBB2 protein (38). p.W151C in exon 6 disrupts the solubility of CRYBB2 and causes abnormal

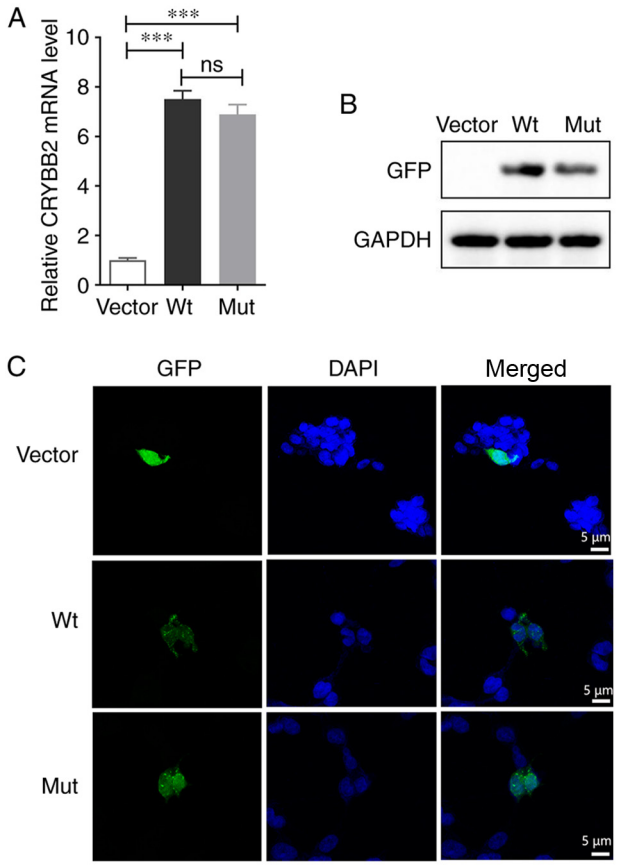

Figure 5. Expression levels of Wt and Mut-*CRYBB2*. (A) Wt-*CRYBB2* and Mut-*CRYBB2* were successfully expressed in transfected cells. Values are presented as the mean ± SD. One-way ANOVA and Bonferroni multiple comparison was used to test the differences between three groups, ***P<0.001. (B) Mut-*CRYBB2* protein expression levels were lower than those of Wt-*CRYBB2* in transfected cells. GAPDH was used as the loading control. (C) Confocal laser scanning images showed that the Mut-*CRYBB2* protein tended to surround the nucleus. Scale bar, 5 μm. *CRYBB2*, β-crystallin B2; Wt, wild-type; Mut, mutant; ns, no significance; GFP, green fluorescent protein.

aggregation of the protein to form membrane cataracts (39). In addition, the p.W151C variant identified in an Indian family was also predicted to disrupt the fourth GKM and increase the protein's hydrophobicity, thereby leading to the formation of cataracts (40). p.Q155X in exon 6 results in a partially unfolded structure and decreased structural order, inhibiting interactions with other proteins (41). p.A188H in exon 6 is a rare variant at the carboxyl terminus, which impairs the dimerization of the CRYBB2 protein by establishing a new hydrogen bond, thereby leading to increased lens opacity (42). Xu *et al* (7) reported that p.A188H caused congenital cataracts and progressive eye axis extension in a five-generation Chinese family. p.I21N in exon 3 is located in the first GKM, on the verge of the N-terminal translation initiation region, which is highly conserved based on multi-species sequence analysis. The N-terminal sequence of a protein has a significant impact on the biological function of the protein; almost all protein synthesis starts at the N-terminus, thus the sequence composition of the N-terminus of the protein has a significant influence on the overall biological function of the protein (43). For example, the N-terminal sequence affects the half-life of the protein (44), and regulates the location of the protein in subcellular organelles (45), which are closely associated with the function and stability of the protein. Song *et al* (46) reported that a heterozygous variant c.35G>T in exon 1 of α-crystallin A chain (CRYAA), located at the N-terminus of the CRYAA protein, induced congenital cataracts and microphthalmia in a four-generation Chinese family, which also illustrated the influence of the stability of the N-terminus on protein function. The N- and C-terminal regions of CRYBB2 have been hypothesized to be essential for the maintenance of lens transparency (47).

CRYBB2:c.62T>A (p.I21N) was also determined to be potentially detrimental by PolyPhen-2 and SIFT. p.I21N was considered as 'probably damaging' and 'deleterious' by PolyPhen-2 and SIFT, respectively. In addition, ProtScale indicated that the hydrophobicity of the mutation site was significantly reduced. Pymol predicted that this variant caused the α-helix located in the first GKM to be replaced by a β-strand, and this change also affected the correct folding of the protein. This change may also explain why this variant protein lost its function, consistent with an earlier report (11). There are a large number of molecular connections between the amino acids in the protein, including various forces and hydrogen bonds. Changes in the hydrophobicity of a certain amino acid site may affect the secondary and tertiary structure of a protein (8,9). The change in the structure of this variant of *CRYBB2* shown by Pymol may have been due to the variant amino acid site exerting effects on the forces of the surrounding amino acids. The resulting conformation re-formed in order to adapt to protein folding. Any mutation that affects a molecule's inner connections can alter a protein's stability and capacity to bind to other proteins. In addition, it has been reported that the lens thermal balance and the ability to resist oxidative stress in the *CRYBB2* gene knockout mice are reduced, which leads to the occurrence of cataracts in mice (48).

Gene therapy for diseases caused by genetic defects is being developed and constantly improved (11), so it is necessary to investigate the mechanisms via which certain gene mutations may cause cataracts. In the present study, the variant discovered was a recurrent pathological variant. It was suggested that the site where the variant was located was likely to be a mutation hotspot or a susceptible site. Hence, gene recombination technology was used to construct mutant and Wt plasmid-transfected cells to assess the possible pathological mechanisms of *CRYBB2*:c.62T>A(p.I21N) in inducing cataracts. Post-transfection, the mRNA expression levels of Wt- and I21N-*CRYBB2* were not altered, suggesting that the variant does not affect transcription, but at the protein levels, the expression levels of I21N-*CRYBB2* were lower than in the Wt-*CRYBB2* transfected cells, suggesting that there may be other processes involved in the regulation of translation, which leads to decreased protein expression. Post-translational modifications of proteins are an important mechanism for maintaining the homeostasis of protein functions in the body (49). Although it is generally hypothesized that congenital cataracts are a single-gene disease (14), complex clinical and genetic heterogeneity is always observed. In the process of gene transcription and translation, a variety of transcription modifiers and protein translation regulation mechanisms are involved (50), which complicates the search for a potential target for clinical therapeutics in diseases caused by gene defects.

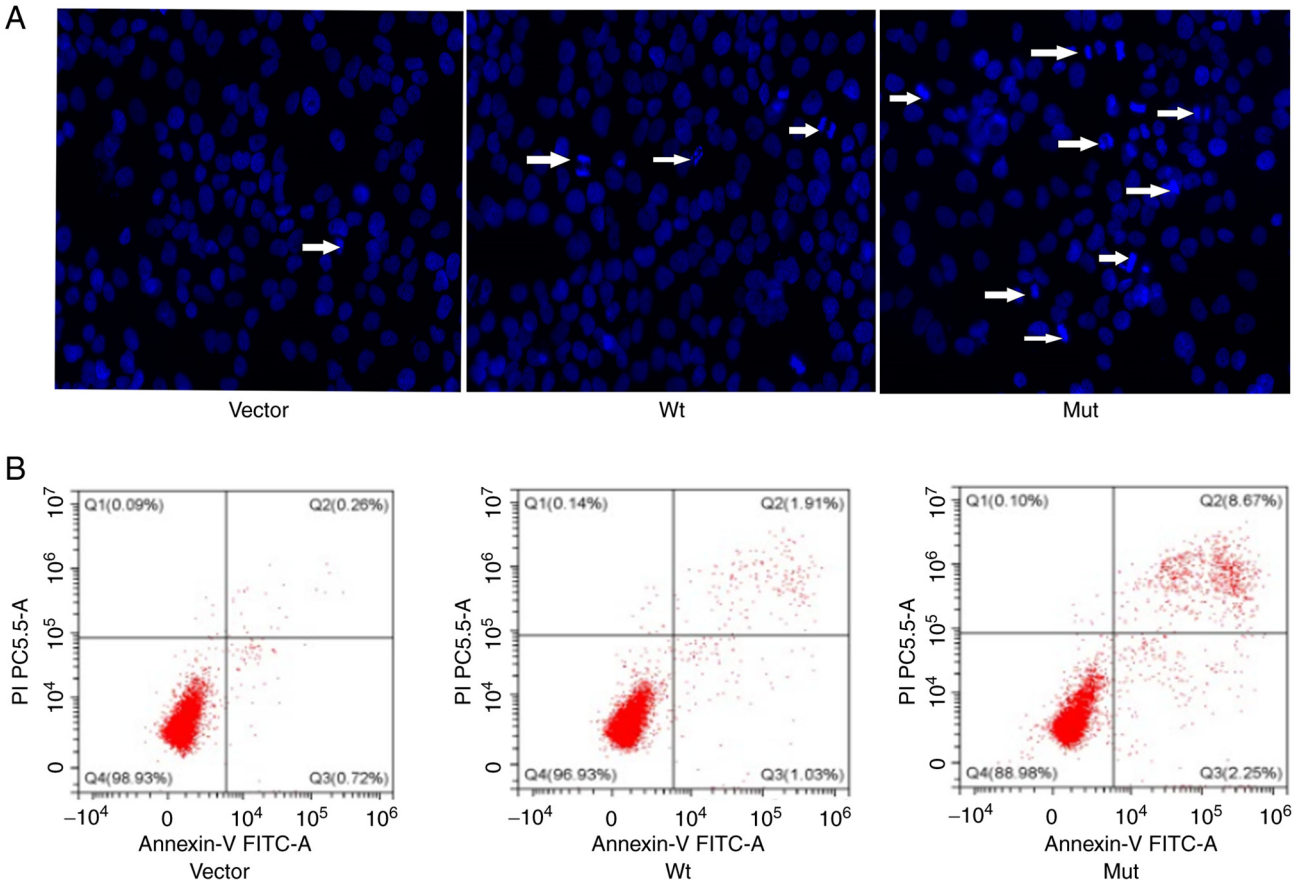

Figure 6. Hoechst 33342 staining and flow cytometry analysis. (A) Hoechst 33342 staining showed increased apoptosis of cells transfected with the variant CRYBB2. The white arrow indicates an apoptotic cell. Magnification, x200. (B) Flow cytometry analysis demonstrated increased apoptosis in cells transfected with the variant CRYBB2. CRYBB2, β-crystallin B2; Wt, wild-type.

In the present study, the immunofluorescence analysis demonstrated that Wt-*CRYBB2* protein predominantly accumulated in the cytoplasm. However, the I21N-*CRYBB2* protein was notably more likely to accumulate around the nucleus. It is hypothesized that the accumulation of these abnormal proteins around the nucleus may prevent the denucleation process of lens fiber cells, thereby destroying the normal lens fiber cells, which are required to maintain lens transparency, resulting in turbidity in the lens (51). Additionally, flow cytometry analysis indicated that the variant may cause cells to be more prone to apoptosis. This may also be an element in the formation of cataracts.

The UPR has been shown to be involved in the pathological process of cataracts caused by certain gene mutations (52). The UPR is considered to be a stress response of cells to stimuli (53). When incorrectly folded proteins are synthesized, they can be terminated in advance or degraded (30), with the aim of preventing abnormal protein accumulation, which can cause damage to cells. There are reports demonstrating the important purpose of the UPR-related genes for a response to a misfolding protein (54-57). For instance, *CRYBB2*: p.V146L was reported to induce cell apoptosis by activating the UPR, resulting in cataracts (9). It has been shown that the abnormal expression of the protein leads to the activation of transcription factors associated with the UPR, which initiates the UPR in an all-round way, and this leads to the apoptosis of fibroblasts (58). In the present study, it was also found that the *CRYBB2*:p.I21N variant induced activation of the UPR, and this led to increased apoptosis of the transfected cells; the present study findings consolidates these previous studies (9), and supports the hypothesis that the activation of the UPR induces partial cataracts.

The formation of cataracts in this family may be caused by abnormal an abnormal N-terminal structure and in the first GKM of the protein in I21N-*CRYBB2*, which does not hinder transcription and translation. However, abnormal N-terminal products may affect the half-life of the protein and also affect the normal anchoring of proteins (59,60) The aggregation of abnormal proteins activates the UPR, which leads to a decrease in the aggregation of abnormal proteins (30). The original purpose may be a protective mechanism, but the activation of UPR also increases the risk of the cell apoptosis. The accumulation of several factors may have thus finally lead to the formation of nuclear cataracts in this four-generation Chinese family.

In conclusion, in the present study, a recurrent variant, *CRYBB2*:c.62T>A(p.I21N), in a four-generation Chinese family with congenital nuclear cataracts was identified using WES, and the effects of this mutation were assessed *in vitro*. These results provide novel evidence via which *CRYBB2*:p.I21N may cause congenital nuclear cataracts. Specifically, the variant exhibited an abnormal N-terminal structure and in the first GKM in the protein, which likely caused the abnormal protein aggregation, that triggered the UPR, induced excessive cell apoptosis, and thus gave rise to the occurrence of congenital nuclear cataracts in this four-generation Chinese family.

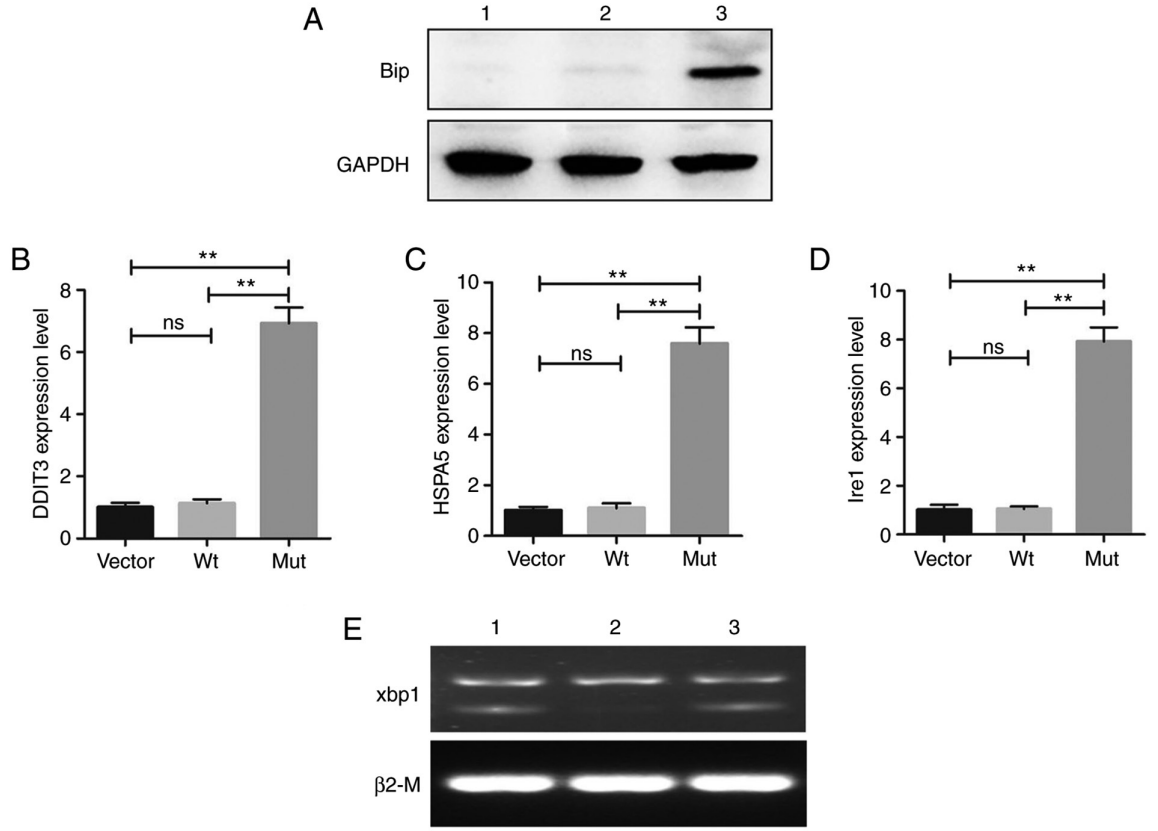

Figure 7. UPR-associated gene expression status in cells. (A) Western blot analysis confirmed the increase in BiP expression in cells expressing the Mut-*CRYBB2*. GAPDH was used as the loading control. Relative mRNA expression levels of (B) *DDIT3*, (C) *HSPA5* and (D) *IRE1*. Values are presented as the mean ± SD. One way ANOVA and Bonferroni multiple comparison was used to test the differences between three groups. **P<0.01. (E) Xbp1 splicing detection (1, Vector; 2, cells expressing Wt-*CRYBB2*; 3, cells expressing Mut-*CRYBB2*). BiP, binding immunoglobulin protein; *DDIT3*, DNA damage-inducible transcript 3; *Ire1*, inositol-requiring enzyme 1; *Xbp1*, X-box-binding protein 1; *HSPA5*, heat shock protein family A (Hsp70) member 5; ns, not significance; Wt, wild-type; Mut, mutant.

Acknowledgements

Not applicable.

Funding

The present study was supported by the National Natural Science Foundation of China (grant no. 51573101), Beijing Natural Science Foundation (grant no. 7172056) and the Xinglin Scholar Scientific Research Promotion Program of Chengdu University of Traditional Chinese Medicine (grant no. BSH2019025).

Availability of data and materials

The datasets generated and/or analyzed during the current study are not publicly available due to the patient privacy protection and local policy (Regulations of the People's Republic of China on the Management of Human Genetic Resources, State Order no. 717) prohibiting data sharing but are available from the corresponding author on reasonable request.

Authors' contributions

DDC performed the molecular genetic study, participated in the sequence alignment and drafted the manuscript. DDC also prepared the figures, edited the manuscript and drafted the molecular results. SQZ conceived the study, participated in its design and coordination and drafted the manuscript. Both authors read and approved the final manuscript. SQZ and DDC checked the data and approved the authenticity of the raw data.

Ethics approval and consent to participate

The study protocol was approved by the Yin Hai Eye Hospital affiliated with Chengdu University of Traditional Chinese Medicine Ethics Committee (Chengdu, China; approval no. CMEC2010-21). Written informed consent was obtained from the participants or their guardians for genetic testing.

Patient consent for publication

Written informed consent was obtained from the participants or their guardians for publication of clinical and genetic data and images.

Competing interests

The authors declare that they have no competing interests.

References

1. Naz S, Sharif S, Badar H, Rashid F, Kaleem A and Iqtedar M: Incidence of environmental and genetic factors causing congenital cataract in children of Lahore. J Pak Med Assoc 66: 819-822, 2016.

2. Li J, Chen X, Yan Y and Yao K: Molecular genetics of congenital cataracts. Exp Eye Res 191: 107872, 2020.
3. Lhussiez V, Dubus E, Cesar Q, Acar N, Nandrot EF, Simonutti M, Audo I, Lizé E, Nguyen S, Geissler A, *et al*: Cohen syndrome-associated cataract is explained by VPS13B functions in lens homeostasis and is modified by additional genetic factors. Invest Ophthalmol Vis Sci 61: 18, 2020.
4. Sheeladevi S, Lawrenson JG, Fielder AR and Suttle CM: Global prevalence of childhood cataract: A systematic review. Eye (Lond) 30: 1160-1169, 2016.
5. Zhuang J, Cao Z, Zhu Y, Liu L, Tong Y, Chen X, Wang Y, Lu C, Ma X and Yang J: Mutation screening of crystallin genes in Chinese families with congenital cataracts. Mol Vis 25: 427-437, 2019.
6. Gerasimovich ES, Strelkov SV and Gusev NB: Some properties of three αB-crystallin mutants carrying point substitutions in the C-terminal domain and associated with congenital diseases. Biochimie 142: 168-178, 2017.
7. Xu LJ, Lv ZG, Liu Y, Zhang XX, Cui YX, Li XC, Zhu YJ and He J: A novel CRYBB2 mutation causes autosomal dominant cataract: A report from a Chinese family. Eur J Ophthalmol 4: 1120672120926450, 2020.
8. Chen W, Chen X, Hu Z, Lin H, Zhou F, Luo L, Zhang X, Zhong X, Yang Y, Wu C, *et al*: A missense mutation in CRYBB2 leads to progressive congenital membranous cataract by impacting the solubility and function of βB2-crystallin. PLoS One 8: e81290, 2013.
9. Li L, Fan DB, Zhao YT, Li Y, Kong DQ, Cai FF and Zheng GY: Two novel mutations identified in ADCC families impair crystallin protein distribution and induce apoptosis in human lens epithelial cells. Sci Rep 7: 17848, 2017.
10. Guo W, Lai Y, Yan Z, Wang Y, Nie Y, Guan S, Kuo Y, Zhang W, Zhu X, Peng M, *et al*: Trio-whole-exome sequencing and preimplantation genetic diagnosis for unexplained recurrent fetal malformations. Hum Mutat 41: 432-448, 2020.
11. Wang KJ, Wang BB, Zhang F, Zhao Y, Ma X and Zhu SQ: Novel beta-crystallin gene mutations in Chinese families with nuclear cataracts. Arch Ophthalmol 129: 337-343, 2011.
12. World Medical Association: World medical association declaration of Helsinki: Ethical principles for medical research involving human subjects. JAMA 310: 2191-2194, 2013.
13. Chun SM, Sung CO, Jeon H, Kim TI, Lee JY, Park H, Kim Y, Kim D and Jang SJ: Next-generation sequencing using S1 nuclease for poor-quality formalin-fixed, paraffin-embedded tumor specimens. J Mol Diagn 20: 802-811, 2018.
14. Zhao S, Zhang C, Mu J, Zhang H, Yao W, Ding X, Ding J and Chang Y: All-in-one sequencing: An improved library preparation method for cost-effective and high-throughput next-generation sequencing. Plant Methods 16: 74, 2020.
15. Li H and Durbin R: Fast and accurate short read alignment with burrows-wheeler transform. Bioinformatics 25: 1754-1760, 2009.
16. Broad Institute: Picard Tools. http://broadinstitute.github.io/picard/. Accessed September 10, 2019.
17. Van der Auwera GA, Carneiro MO, Hartl C, Poplin R, Del Angel G, Levy-Moonshine A, Jordan T, Shakir K, Roazen D, Thibault J, *et al*: From FastQ data to high confidence variant calls: The genome analysis toolkit best practices pipeline. Curr Protoc Bioinformatics 43: 11.10.1-11.10.33, 2013.
18. Wang K, Li M and Hakonarson H: ANNOVAR: Functional annotation of genetic variants from high-throughput sequencing data. Nucleic Acids Res 38: e164, 2010.
19. Kumar P, Henikoff S and Ng PC: Predicting the effects of coding non-synonymous variants on protein function using the SIFT algorithm. Nat Protoc 4: 1073-1081, 2009.
20. Adzhubei IA, Schmidt S, Peshkin L, Ramensky VE, Gerasimova A, Bork P, Kondrashov AS and Sunyaev SR: A method and server for predicting damaging missense mutations. Nat Methods 7: 248-249, 2010.
21. Schwarz JM, Cooper DN, Schuelke M and Seelow D: MutationTaster2: Mutation prediction for the deep-sequencing age. Nat Methods 11: 361-362, 2014.
22. Cooper GM, Stone EA, Asimenos G, NISC Comparative Sequencing Program; Green ED, Batzoglou S and Sidow A: Distribution and intensity of constraint in mammalian genomic sequence. Genome Res 15: 901-913, 2005.
23. ACMG Board Of Directors: ACMG policy statement: Updated recommendations regarding analysis and reporting of secondary findings in clinical genome-scale sequencing. Genet Med 17: 68-69, 2015.
24. Richards S, Aziz N, Bale S, Bick D, Das S, Gastier-Foster J, Grody WW, Hegde M, Lyon E, Spector E, *et al*: Standards and guidelines for the interpretation of sequence variants: A joint consensus recommendation of the American college of medical genetics and genomics and the association for molecular pathology. Genet Med 17: 405-424, 2015.
25. Seeliger D and de Groot BL: Ligand docking and binding site analysis with PyMOL and autodock/vina. J Comput Aided Mol Des 24: 417-422, 2010.
26. Balaji S and Vanniarajan A: Implication of pseudo reference genes in normalization of data from reverse transcription-quantitative PCR. Gene 757: 144948, 2020.
27. Livak KJ and Schmittgen TD: Analysis of relative gene expression data using real-time quantitative PCR and the 2(-Delta Delta C(T)) method. Methods 25: 402-408, 2001.
28. Mooers B: Shortcuts for faster image creation in PyMOL. Protein Sci 29: 268-276, 2020.
29. Hetz C and Papa FR: The unfolded protein response and cell fate control. Mol Cell 69: 169-181, 2018.
30. Bashir S, Banday M, Qadri O, Bashir A, Hilal N, Nida-I-Fatima, Rader S and Fazili KM: The molecular mechanism and functional diversity of UPR signaling sensor IRE1. Life Sci 265: 118740, 2021.
31. Sharma RB, Darko C and Alonso LC: Intersection of the ATF6 and XBP1 ER stress pathways in mouse islet cells. J Biol Chem 295: 14164-14177, 2020.
32. Berry V, Georgiou M, Fujinami K, Quinlan R, Moore A and Michaelides M: Inherited cataracts: Molecular genetics, clinical features, disease mechanisms and novel therapeutic approaches. Br J Ophthalmol 104: 1331-1337, 2020.
33. Liu H, Wei X, Sha Y, Liu W, Gao H, Lin J, Li Y, Tang Y, Wang Y, Wang Y and Su Z: Whole-exome sequencing in patients with premature ovarian insufficiency: Early detection and early intervention. J Ovarian Res 13: 114, 2020.
34. Astiazarán MC, García-Montaño LA, Sánchez-Moreno F, Matiz-Moreno H and Zenteno JC: Next generation sequencing-based molecular diagnosis in familial congenital cataract expands the mutational spectrum in known congenital cataract genes. Am J Med Genet A 176: 2637-2645, 2018.
35. Hwang SS, Kim WS and Lee SJ: Clinical features of strabismus and nystagmus in bilateral congenital cataracts. Int J Ophthalmol 11: 813-817, 2018.
36. Magli A, Carelli R, Forte R, Vecchio EC, Esposito F and Torre A: Congenital and developmental cataracts: Focus on strabismus outcomes at long-term follow-up. Semin Ophthalmol 32: 358-362, 2017.
37. Kuhli-Hattenbach C, Fronius M and Kohnen T: Timing of congenital cataract surgery: Amblyopia versus aphakic glaucoma. Ophthalmologe 117: 190-198, 2020 (In German).
38. Pauli S, Söker T, Klopp N, Illig T, Engel W and Graw J: Mutation analysis in a German family identified a new cataract-causing allele in the CRYBB2 gene. Mol Vis 13: 962-967, 2007.
39. Zhao WJ, Xu J, Chen XJ, Liu HH, Yao K and Yan YB: Effects of cataract-causing mutations W59C and W151C on βB2-crystallin structure, stability and folding. Int J Biol Macromol 103: 764-770, 2017.
40. Santhiya ST, Manisastry SM, Rawlley D, Malathi R, Anishetty S, Gopinath PM, Vijayalakshmi P, Namperumalsamy P, Adamski J and Graw J: Mutation analysis of congenital cataracts in Indian families: Identification of SNPS and a new causative allele in CRYBB2 gene. Invest Ophthalmol Vis Sci 45: 3599-3607, 2004.
41. Li FF, Zhu SQ, Wang SZ, Gao C, Huang SZ, Zhang M and Ma X: Nonsense mutation in the CRYBB2 gene causing autosomal dominant progressive polymorphic congenital coronary cataracts. Mol Vis 14: 750-755, 2008.
42. Weisschuh N, Aisenbrey S, Wissinger B and Riess A: Identification of a novel CRYBB2 missense mutation causing congenital autosomal dominant cataract. Mol Vis 18: 174-180, 2012.
43. Kim L, Kwon DH, Heo J, Park MR and Song HK: Use of the LC3B-fusion technique for biochemical and structural studies of proteins involved in the N-degron pathway. J Biol Chem 295: 2590-2600, 2020.
44. Friemel M, Marelja Z, Li K and Leimkühler S: The N-terminus of iron-sulfur cluster assembly factor ISD11 is crucial for subcellular targeting and interaction with l-cysteine desulfurase NFS1. Biochemistry 56: 1797-1808, 2017.
45. Skach WR, Shi LB, Calayag MC, Frigeri A, Lingappa VR and Verkman AS: Biogenesis and transmembrane topology of the CHIP28 water channel at the endoplasmic reticulum. J Cell Biol 125: 803-815, 1994.

46. Song Z, Si N and Xiao W: A novel mutation in the CRYAA gene associated with congenital cataract and microphthalmia in a Chinese family. BMC Med Genet 19: 190, 2018.
47. Carver JA, Grosas AB, Ecroyd H and Quinlan RA: The functional roles of the unstructured N- and C-terminal regions in αB-crystallin and other mammalian small heat-shock proteins. Cell Stress Chaperones 22: 627-638, 2017.
48. Zhang J, Li J, Huang C, Xue L, Peng Y, Fu Q, Gao L, Zhang J and Li W: Targeted knockout of the mouse betaB2-crystallin gene (Crybb2) induces age-related cataract. Invest Ophthalmol Vis Sci 49: 5476-5483, 2008.
49. Song L and Luo ZQ: Post-translational regulation of ubiquitin signaling. J Cell Biol 218: 1776-1786, 2019.
50. Frye M, Harada BT, Behm M and He C: RNA modifications modulate gene expression during development. Science 361: 1346-1349, 2018.
51. Zhang J, Cui WW, Du C, Huang Y, Pi X, Guo W, Wang J, Huang W, Chen D, Li J, *et al*: Knockout of DNaseIIl1 abrogates lens denucleation process and causes cataract in zebrafish. Biochim Biophys Acta Mol Basis Dis 1866: 165724, 2020.
52. Shiels A and Hejtmancik JF: Inherited cataracts: Genetic mechanisms and pathways new and old. Exp Eye Res 209: 108662, 2021.
53. Chan WC, Tsang KY, Cheng YW, Ng VC, Chik H, Tan ZJ, Boot-Handford R, Boyde A, Cheung KN, Cheah KS and Chan D: Activating the unfolded protein response in osteocytes causes hyperostosis consistent with craniodiaphyseal dysplasia. Hum Mol Genet 26: 4572-4587, 2017.
54. Berry V, Pontikos N, Moore A, Ionides A, Plagnol V, Cheetham ME and Michaelides M: A novel missense mutation in HSF4 causes autosomal-dominant congenital lamellar cataract in a British family. Eye (Lond) 32: 806-812, 2018.
55. Ghavami S, Yeganeh B, Zeki AA, Shojaei S, Kenyon NJ, Ott S, Samali A, Patterson J, Alizadeh J, Moghadam AR, *et al*: Autophagy and the unfolded protein response promote profibrotic effects of TGF-β(1) in human lung fibroblasts. Am J Physiol Lung Cell Mol Physiol 314: L493-L504, 2018.
56. Schinzel RT, Higuchi-Sanabria R, Shalem O, Moehle EA, Webster BM, Joe L, Bar-Ziv R, Frankino PA, Durieux J, Pender C, *et al*: The hyaluronidase, TMEM2, promotes ER homeostasis and longevity independent of the UPR ER. Cell 179: 1306-1318, 2019.
57. Muñoz JP, Ivanova S, Sánchez-Wandelmer J, Martínez-Cristóbal P, Noguera E, Sancho A, Díaz-Ramos A, Hernández-Alvarez MI, Sebastián D, Mauvezin C, *et al*: Mfn2 modulates the UPR and mitochondrial function via repression of PERK. EMBO J 32: 2348-2361, 2013.
58. Andley UP and Goldman JW: Autophagy and UPR in alpha-crystallin mutant knock-in mouse models of hereditary cataracts. Biochim Biophys Acta 1860: 234-239, 2016.
59. Nguyen KT, Lee CS, Mun SH, Truong NT, Park SK and Hwang CS: N-terminal acetylation and the N-end rule pathway control degradation of the lipid droplet protein PLIN2. J Biol Chem 294: 379-388, 2019.
60. Nguyen KT, Mun SH, Lee CS and Hwang CS: Control of protein degradation by N-terminal acetylation and the N-end rule pathway. Exp Mol Med 50: 1-8, 2018.

This work is licensed under a Creative Commons Attribution-NonCommercial-NoDerivatives 4.0 International (CC BY-NC-ND 4.0) License.